

Special Section:

Southern Ocean and Climate:
Biogeochemical and Physical
Fluxes and Processes

Key Points:

- Current-wind interaction reduces CO₂ outgassing by 17% in the Pacific sector of the Southern Ocean
- Weaker vertical mixing lowers the partial pressure of CO₂ (pCO₂) to the south of the northern subantarctic front
- The weaker wind stress and Ekman transport also assist in lowering pCO₂

Supporting Information:

Supporting Information may be found in the online version of this article.

Correspondence to:

H. Song,
hajsong@yonsei.ac.kr

Citation:

Kwak, K., Song, H., Marshall, J., Seo, H., & McGillicuddy, D. J. Jr. (2021). Suppressed pCO₂ in the Southern Ocean due to the interaction between current and wind. *Journal of Geophysical Research: Oceans*, 126, e2021JC017884. <https://doi.org/10.1029/2021JC017884>

Received 12 AUG 2021

Accepted 12 NOV 2021

Suppressed pCO₂ in the Southern Ocean Due to the Interaction Between Current and Wind

Kyungmin Kwak¹ , Hajoon Song¹ , John Marshall² , Hyodae Seo³ , and Dennis J. McGillicuddy Jr⁴ 

¹Department of Atmospheric Sciences, Yonsei University, Seoul, Republic of Korea, ²Department of Earth, Atmospheric and Planetary Sciences, Massachusetts Institute of Technology, Cambridge, MA, USA, ³Physical Oceanography Department, Woods Hole Oceanographic Institution, Woods Hole, MA, USA, ⁴Department of Applied Ocean Physics and Engineering, Woods Hole Oceanographic Institution, Woods Hole, MA, USA

Abstract The Southern Ocean, an important region for the uptake of anthropogenic carbon dioxide (CO₂), features strong surface currents due to substantial mesoscale meanders and eddies. These features interact with the wind and modify the momentum transfer from the atmosphere to the ocean. Although such interactions are known to reduce momentum transfer, their impact on air-sea carbon exchange remains unclear. Using a 1/20° physical-biogeochemical coupled ocean model, we examined the impact of the current-wind interaction on the surface carbon concentration and the air-sea carbon exchange in the Southern Ocean. The current-wind interaction decreased winter partial pressure of CO₂ (pCO₂) at the ocean surface mainly south of the northern subantarctic front. It also reduced pCO₂ in summer, indicating enhanced uptake, but not to the same extent as the winter loss. Consequently, the net outgassing of CO₂ was found to be reduced by approximately 17% when including current-wind interaction. These changes stem from the combined effect of vertical mixing and Ekman divergence. A budget analysis of dissolved inorganic carbon (DIC) revealed that a weakening of vertical mixing by current-wind interaction reduces the carbon supply from below, and particularly so in winter. The weaker wind stress additionally lowers the subsurface DIC concentration in summer, which can affect the vertical diffusive flux of carbon in winter. Our study suggests that ignoring current-wind interactions in the Southern Ocean can overestimate winter CO₂ outgassing.

Plain Language Summary The Southern Ocean, subjected to strong winds and exhibiting highly energetic, eddying flows, is a key region for air-sea exchange of carbon dioxide (CO₂). Although the impacts on ocean circulation and mesoscale energetics by current-wind interaction are beginning to be better understood, it remains unclear how the interaction between the wind and ocean eddies modulates the CO₂ exchange. Using a 1/20° physical-biogeochemical coupled ocean model, we analyze changes in air-sea CO₂ flux induced by current-wind interaction. The interaction reduces CO₂ outgassing in winter and slightly increases CO₂ uptake in spring, leading to a 17% reduction in the net CO₂ outgassing. The changes are observed mainly to the south of approximately 55°S. Detailed analysis reveals that the suppression of CO₂ outgassing by current-wind coupling is mainly the result of weaker vertical mixing along with reduced upwelling, which decreases the carbon concentration at the surface. Our study suggests that ignoring the current-wind interaction in the Southern Ocean can significantly overestimate CO₂ outgassing.

1. Introduction

The energy input by wind is the greatest in the Southern Ocean (Belmonte Rivas & Stoffelen, 2019; Huang et al., 2006; Wunsch, 1998). The westerly wind transports the surface water equatorward, which forces the upwelling that brings Circumpolar Deep Water to the surface (Marshall & Speer, 2012; Takahashi et al., 2012; Tamsitt et al., 2017). The upwelling in turn contributes to the tilt of isopycnals and formation of Antarctic Circumpolar Current (Allison et al., 2011; Langlais et al., 2015; Wang et al., 2011). A negative wind stress curl to the south of the maximum westerly wind further creates upwelling through surface divergence (Carranza & Gille, 2015; Luis & Pandey, 2004), which allows the deep ocean to interact with the atmosphere (Marshall & Speer, 2012; Sallée, 2018). Excessive precipitation and sea-ice melting over the Southern Ocean reduces the salinity of the upwelled water and shapes the characteristics of the Antarctic Intermediate Water. Newly upwelled water takes up heat from the atmosphere before subducting in the lower latitudes (Abernathy et al., 2016; Durack et al., 2014; Frölicher et al., 2015; Morrison et al., 2016; Roemmich et al., 2015). Indeed, autonomous profiling

floats have shown a continued increase of the heat content in the upper 2,000 m of the Southern Ocean in the last two decades, which can explain the majority of global ocean heat content changes (Llovel & Terray, 2016; Roemmich et al., 2015).

Upwelling and vertical mixing in the Southern Ocean also plays an important role in the exchange of carbon dioxide (CO₂) between the atmosphere and deep ocean. Since the carbon concentration is greater at depth, upwelling increases dissolved inorganic carbon (DIC) at the surface, leading to release of CO₂ to the atmosphere. Simultaneously, the Southern Ocean uptakes a significant amount of anthropogenic carbon from the atmosphere when moving to lower latitudes (Khatiwala et al., 2009; Lenton et al., 2013; Mikaloff Fletcher et al., 2006).

Air-sea CO₂ exchange in the Southern Ocean is a complicated process. First, it is characterized by strong seasonality (Brix et al., 2013; Lenton et al., 2006, 2013; Metzl et al., 2006; Takahashi et al., 2002; Thomalla et al., 2011), stemming from the seasonally varying oceanic partial pressure of CO₂ (*p*CO₂) (Brix et al., 2013; Gruber et al., 2019), with higher values in austral winter than summer. The intense vertical mixing increases the surface *p*CO₂ in winter, whereas it is lowered by enhanced biological activity in spring (Bakker et al., 1997; Gregor et al., 2018; Gruber et al., 2019; Hales & Takahashi, 2004; Person et al., 2018; Takahashi et al., 2002, 2012). Since the CO₂ flux is determined by the *p*CO₂ difference between the atmosphere and the ocean (Wanninkhof, 1992), the Southern Ocean tends to release CO₂ to the atmosphere in winter but exhibits CO₂ uptake in summer. Second, CO₂ flux displays a latitudinal dependency. An estimation based on autonomous biogeochemical floats suggests year-round CO₂ uptake in the subtropical zone and significant CO₂ outgassing between the polar front and the seasonal sea-ice extent (Gray et al., 2018). In other latitudinal bands, the direction of CO₂ fluxes changes from CO₂ uptake in summer to outgassing in winter, although their magnitudes differ. If other data products are considered, the CO₂ flux values diverge from the float data outside of the error bars in some cases (Le Quére et al., 2018; Takahashi et al., 2009), possibly due to the scarcity of *p*CO₂ observations.

Air-sea interaction in the oceanic mesoscale can impose another layer of complexity to CO₂ exchange in the Southern Ocean. A recent observational study by Pezzi et al. (2021) reports that a warm-core eddy in the southwestern Atlantic Ocean acts as a local source of CO₂ to the atmosphere in contrast to the surrounding cold waters, which are considered as a sink. The sea surface temperature perturbation associated with the mesoscale modifies the surface wind speed (Chelton et al., 2007; Putrasahan et al., 2013; Samelson et al., 2006; Seo et al., 2007), which can alter the air-sea CO₂ exchange. Also, according to the bulk formulae, the surface wind stress can be estimated using the difference between the wind at 10 m and the surface ocean current (Large & Yeager, 2004). Since the surface current is significantly smaller than that of the wind, it is often neglected in the wind stress calculation. However, previous studies reported considerable changes in the mesoscale activities by “top drag” effects of the ocean when the surface current is included in the calculation (Dawe & Thompson, 2006; Dewar & Flierl, 1987; Duhaut & Straub, 2006; Eden & Dietze, 2009; Martin & Richards, 2001; Zhai et al., 2012). In particular, this current-wind interaction, commonly known as the relative wind (RW) effect, leads to the reduction of eddy kinetic energy (EKE) by at least 10% and as much as 100% depending on the geographic location (Jullien et al., 2020; Renault et al., 2016; Seo, 2017; Seo et al., 2016, 2019; Zhai & Greatbatch, 2007). In the Southern Ocean, the RW effect could reduce EKE by approximately 11%–25% (Hutchinson et al., 2010; Song et al., 2020).

The impacts of RW on biogeochemical properties have also been discussed in previous studies. Inclusion of the surface current creates a wind stress curl over the mesoscale eddies, which results in additional vertical motion (Gaubert et al., 2015), along with anomalous nutrient fluxes and chlorophyll concentrations (Anderson et al., 2011; Ledwell et al., 2008; McGillicuddy et al., 2007). However, the vertical motion triggered by the wind stress curl is weaker than that associated with mesoscale or submesoscale processes (Lévy et al., 2001), which also alters biogeochemical processes such as primary production, biogeochemical fluxes, and community structure (Anderson & Robinson, 2001; Flierl & Davis, 1993; Lévy et al., 2018; Mahadevan & Archer, 2000; Smith et al., 1996; Yoshimori & Kishi, 1994). Indeed, Eden and Dietze (2009) performed numerical simulations over the North Atlantic Ocean showing that the inclusion of surface current in the stress calculation does not significantly change the production or CO₂ flux.

The minimal impact of the RW effect on CO₂ flux in the North Atlantic (Eden & Dietze, 2009) may not be applicable to the Southern Ocean because they are considerably different with respect to the physical mechanisms controlling the biogeochemical properties. The cold temperature and predominant upwelling driven by wind in the Southern Ocean increases the DIC concentration at the surface (Wu et al., 2019). In contrast, the North

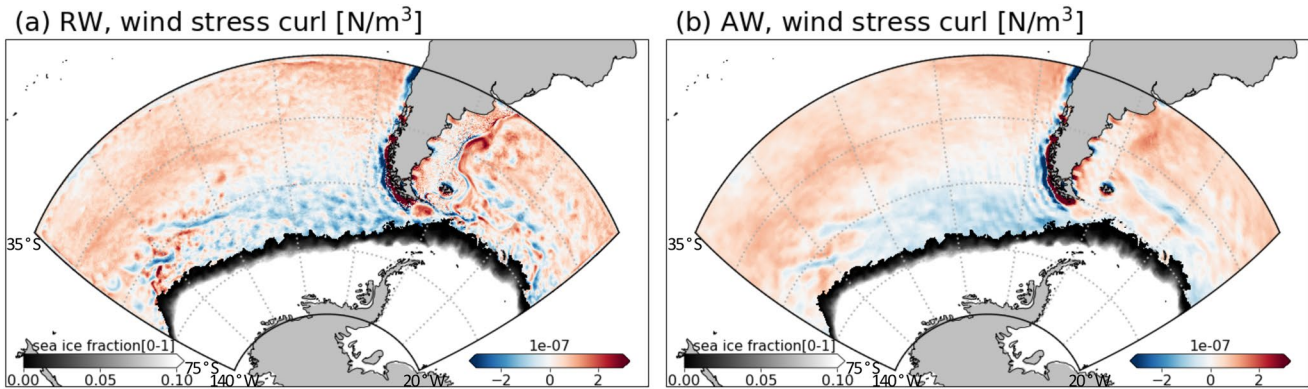


Figure 1. Annual mean wind stress curl in (a) RW and (b) AW. Sea-ice fractions are indicated by the gray scale.

Atlantic can be characterized by downwelling in the subtropical gyre from the surface convergence. Although the subpolar gyre has upwelling, it does not extend deeper than 1,000 m (Liang et al., 2017). Consequently, the spatially averaged concentration of DIC in the North Atlantic is lower than that in the Southern Ocean at all depths (Olsen et al., 2020). The vertical gradient of the DIC concentration near the surface, which depends on location, also needs to be considered when discussing the impact of the RW on the CO₂ flux.

The above argument raises a question as to whether the RW effect can alter CO₂ flux in the Southern Ocean, which plays a critical role in the carbon cycle. To address this question, we investigated the impact of the RW effect on the CO₂ flux using a physical-biogeochemical coupled ocean model configured in the Southern Ocean near the Drake Passage. This model showed that the RW stress tends to reduce the surface *p*CO₂, in particular near the south of the northern subantarctic front (nSAF) in all months, resulting in reduced net CO₂ outgassing. A DIC budget analysis was further applied to quantify the contributions from varied processes, including advection, diffusion, and biological sink. The overall result shows that the changes in the air-sea CO₂ exchange were found to be sizable in spite of the relatively small modification of wind stress by the RW effect, demonstrating acute sensitivity of the air-sea CO₂ exchanges to small variation in SO wind fields.

This paper is organized as follows. The configuration of eddy-resolving physical and biogeochemical coupled model and the experimental settings are presented in Section 2. Section 3 shows the resulting air-sea CO₂ exchange in the numerical experiments, which is followed by the analysis of the air-sea CO₂ exchange using DIC and its budget in Section 4. We conclude the study with a discussion in Section 5.

2. Simulation of the Carbon Cycle in the Southern Ocean

2.1. Model Configuration for Carbon Cycle Simulation

Carbon exchange between the atmosphere and the ocean was estimated using a simple biogeochemical model (Dutkiewicz et al., 2005; Parekh et al., 2006; Verdy et al., 2007) embedded in a regional version of the MIT General Circulation Model (MITgcm) (Marshall, Hill, et al., 1997; Marshall, Adcroft, et al., 1997; Adcroft et al., 1997; Marshall et al., 1998; Adcroft et al., 2004). In this biogeochemical model, the source/sink of the carbon cycle consists of six biogeochemical properties. The consumption of carbon in the model is mainly through the marine net community production (NCP) that is estimated using light, nitrate, and iron as follows.

$$\text{NCP} = \alpha \frac{I}{\kappa_I + I} \min \left(\frac{\text{NO}_3}{\kappa_{\text{NO}_3} + \text{NO}_3}, \frac{\text{Fe}}{\kappa_{\text{Fe}} + \text{Fe}} \right), \quad (1)$$

where, α is the maximum community production rate, κ_I , κ_{NO_3} and κ_{Fe} are half saturation number of light (I), nitrate (NO₃), and iron (Fe), respectively. A portion of the NCP is remineralized and transported to the depths, and the remains enter the dissolved organic field. More detailed aspects of this BGC model configuration can be found in a previous study (Song, Marshall, Munro, et al., 2016). The model domain includes the Drake Passage, its upstream and downstream spanning from 160°W to 20°W with a 1/20° interval (Figure 1). The latitudinal range stretched from Antarctica (75°S) to the subtropical gyre (35°S). The Antarctic Circumpolar Current (ACC)

penetrates near the center of the model domain from the southeast Pacific through the Drake Passage to the southwest Atlantic. The ocean was discretized by 50 vertical levels with higher resolution near the surface (10 m). Surface vertical mixing was estimated using K-profile parameterization (KPP) with the critical Richardson number of 0.3583 (Large et al., 1994). The dynamic and thermodynamic properties of the sea-ice at the southern part of the domain were calculated in the sea-ice model (Losch et al., 2010).

The physical and biogeochemical states were initialized using the Ocean Comprehensive Atlas (OCCA, Forget, 2010) and a global spin-up run with approximately 1° resolution (Song, Marshall, Follows, et al., 2016), respectively. These products also provide the monthly averaged boundary conditions, while the ERA-Interim (Dee et al., 2011) forces the ocean from the surface at every 6 h. The surface forcing includes aerial dust input that supplies iron (Luo et al., 2008). Iron is also supplied from the sediment, which was parameterized using the nutrient flux from the bottom layer (Song, Marshall, Munro, et al., 2016). The air-sea carbon exchange, F_{CO_2} , was calculated using the fixed atmospheric pCO_2 (pCO_2^{atm}) to the pre-industrial value (278 ppm), as follows:

$$F_{CO_2} = K_w(1 - A_{SI})(pCO_2^{atm} - pCO_2), \quad (2)$$

where A_{SI} is the sea-ice fraction, K_w is the gas transfer velocity ($m\ s^{-1}$) calculated using wind speed squared and sea surface temperature (SST) (Wanninkhof, 1992). The detailed description of the model configuration can be found in Song et al. (2020).

2.2. Wind Stress Calculation

We investigate the effect of the current-wind interaction on the exchange of CO_2 between the atmosphere and the ocean by comparing two simulations in which only the wind stress calculation differs. The wind stress $\boldsymbol{\tau} = (\tau_x, \tau_y)$ is given by:

$$\boldsymbol{\tau} = \rho_a C_D (\mathbf{u}_a - \beta \mathbf{u}_o) |\mathbf{u}_a - \beta \mathbf{u}_o|, \quad (3)$$

where $\mathbf{u}_a = (u_{a,x}, u_{a,y})$ is the 10 m wind, $\mathbf{u}_o = (u_{o,x}, u_{o,y})$ is the surface current, and ρ_a and C_D are the air density and drag coefficient, respectively. Parameter β was set to 1 in the relative wind simulation (RW) and 0 in the absolute wind simulation (AW). These two simulations are performed for 4 years, in which the first year is considered as the spin-up period and the following three years are analyzed to quantify the impact of the current-wind interaction on the exchange of carbon between the atmosphere and the ocean. Including \mathbf{u}_o in Equation 3 does not significantly change the large-scale wind stress or wind stress curl fields. The difference in the spatially averaged wind stress is less than 3% as $|\mathbf{u}_a| > |\mathbf{u}_o|$. However, the RW effect leaves a footprint from the mesoscale (Figure 1). The RW effect locally enlarges the wind stress curl up by one order of magnitude. The ocean's physical changes from AW to RW runs are presented in Song et al. (2020) with the identical model setup, which can be summarized as follows. The EKE is reduced by approximately 24% even at depths below 500 m. Enhanced stratification is found below the mixing depth that can be attributed to a southward shift of the outcropping latitude for isopycnals in the RW simulation. Local differences in the mixing depth can be greater than 100 m, but the zonally averaged mixing depth calculated by the KPP scheme shows insignificant changes in both summer and winter.

3. Changes in the Air-Sea Exchange of CO_2 by the Current-Wind Interaction

Our simulation captures the seasonal variability of the air-sea CO_2 flux in the Southern Ocean even with rather simple carbon processes (Figure 2a). The upwelling of carbon-rich waters and deep surface mixing in austral winter increased pCO_2 at the surface ocean beyond the atmospheric value, leading to outgassing. This intense mixing can provide iron to the euphotic layer and fuels the biological productivity and carbon consumption when light becomes available in spring. This process consequently leads to the oceanic pCO_2 decrease and facilitates CO_2 uptake by the Southern Ocean. The maximum outgassing is found in winter, with a value of $49\ \text{nmol}\ C\ m^{-2}\ s^{-1}$, which is in the same order of magnitude observed based on biogeochemical floats (Gray et al., 2018).

The interaction between the wind and current shifted the spatially averaged CO_2 flux curve upward, indicating suppressed outgassing (negative CO_2 flux) in winter and enhanced uptake (positive CO_2 flux) in spring (Figure 2a). The largest shift occurs in winter (July-September) when the outgassing is approximately 10% lower in the RW than in the AW (Figure 2b). In the subtropical gyre and near the ACC, the two simulations show a similar

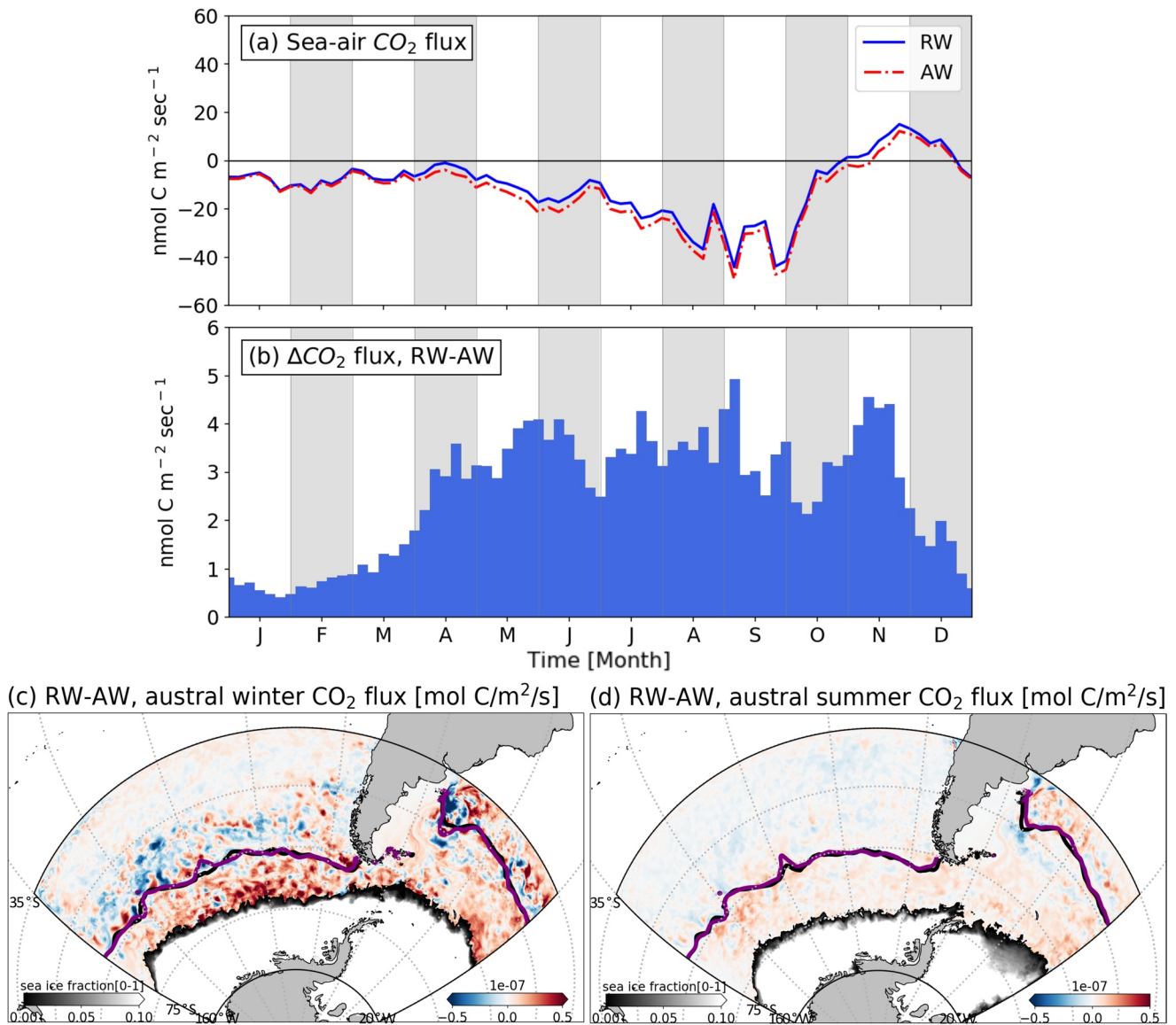


Figure 2. (a) Seasonal cycle of the air-sea CO₂ flux at the surface in the RW (blue solid line) and AW (red dash-dotted line) averaged over three years. Positive and negative values represent the CO₂ uptake (from the atmosphere to the ocean) and outgassing (from the ocean to the atmosphere), respectively. The CO₂ flux differences ($F_{CO_2,RW}-F_{CO_2,AW}$) are shown in (b). The averaged air-sea CO₂ flux differences ($F_{CO_2,RW}-F_{CO_2,AW}$) in (c) winter (July–September) and (d) summer (December–February). The solid lines indicate the smoothed nSAF (black is the RW and purple is the AW) in (c, d). The sea-ice fractions are superimposed in (c, d) in the gray scale.

pattern and size of CO₂ exchange, with enhanced uptake and reduced outgassing, respectively. However, the RW model shows reduced outgassing to the south of nSAF (Figure 2c). By contrast, in summer (December–February), the CO₂ exchanges in the two simulations are almost indistinguishable (Figure 2d). Although the spatial distributions of seasonally averaged CO₂ fluxes in two simulations look similar, the integrated CO₂ exchange over the entire year in the model domain is 0.081 GtC for the AW model, which is reduced by approximately 17% to 0.067 GtC in the RW model. We expect this estimate to be lower than the observed estimate because of the lower atmospheric pCO_2 value chosen in the experiment compared to the present day.

This shift is primarily due to the lower pCO_2 in the RW. Among the variables required in the CO₂ flux calculation by Equation 2, the simulation uses the same wind speed and pCO_2^{atm} values while the SST, sea-ice fraction, and pCO_2 are provided from the models at every time step. The SST changes are subtle between the two simulations (Figure 3c). There is a slight increase in sea-ice concentration in the RW model, resulting in the suppression of the air-sea carbon exchange. However, its impact is limited in the sea-ice area, and the greater uptake in RW in

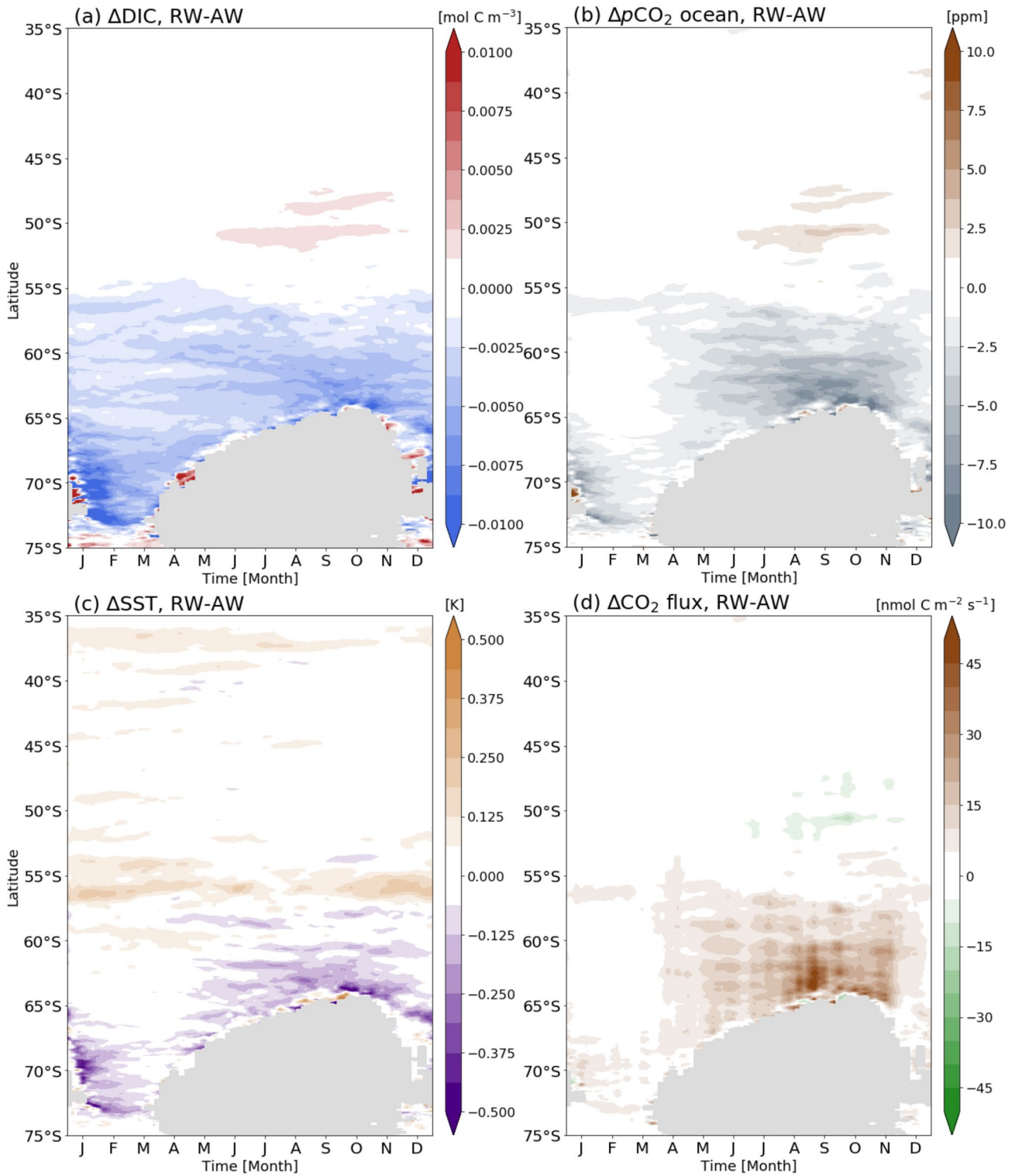


Figure 3. Hovmöller diagrams of the (a) zonally averaged DIC differences ($\text{DIC}_{\text{RW}} - \text{DIC}_{\text{AW}}$), (b) $p\text{CO}_2$ differences ($p\text{CO}_{2,\text{RW}} - p\text{CO}_{2,\text{AW}}$), (c) SST differences ($\text{SST}_{\text{RW}} - \text{SST}_{\text{AW}}$), and (d) CO_2 flux differences ($F_{\text{CO}_2,\text{RW}} - F_{\text{CO}_2,\text{AW}}$) at the surface in the Pacific region of the model domain. Sea-ice covered areas are shown using gray masks.

spring offset the increased sea-ice fraction. Hence, the CO_2 flux reflects the changes in the oceanic $p\text{CO}_2$ changes driven by the current-wind interaction.

4. DIC Changes in the Southern Ocean

4.1. Hovmöller Diagram of DIC

To better understand the spatial temporal dependencies of the CO_2 flux changes by RW, we create a Hovmöller diagram after computing the zonal average of $p\text{CO}_{2,\text{RW}} - p\text{CO}_{2,\text{AW}}$ over the Pacific sector of the model domain (Figure 3b). The largest change is found in the winter months between 55°S and 65°S that is the south of nSAF. A slight increase of $p\text{CO}_2$ in RW occasionally appears to the north of 55°S , but the size of the differences in $p\text{CO}_2$ was insignificant (less than 0.2 ppm) in most cases. In the summer months from January to March the decrease of $p\text{CO}_2$ in RW also appeared in a localized region to the south of 65°S near the sea-ice extent. This Hovmöller diagram (Figure 3b) suggests that the decreased outgassing in RW (Figure 2a) is associated with the decreased $p\text{CO}_2$ near the marginal sea-ice area, especially in the winter months.

We further investigate the changes in DIC to understand the reduced $p\text{CO}_2$ in RW. The current-wind interaction decreases the DIC concentration at the surface in the high latitudes. The Hovmöller diagram shows the decreased DIC level mainly to the south of nSAF (approximately 55°S) (Figure 3a), which is consistent with the $p\text{CO}_2$ changes (Figure 3b). In the winter months, there are visual similarities in the spatial distributions of the changes in DIC and $p\text{CO}_2$ by the RW, suggesting that the reduction of $p\text{CO}_2$ originates from the decrease of DIC. However, the changes in DIC do not correspond to those in $p\text{CO}_2$ in the summer and early fall months (from January to April). In fact, the size of the DIC reduction in RW is slightly greater in summer than in winter, which is the opposite of the case for $p\text{CO}_2$ changes. This is because the $p\text{CO}_2$ changes are influenced by the subtle differences in the SST; cooler SST in RW results in lower $p\text{CO}_2$ near the sea-ice extent in summer. These results are in agreement with previous studies showing that the non-thermal component DIC dominates the $p\text{CO}_2$ in winter, whereas it is primarily driven by the thermal component in summer (Gruber et al., 2019).

4.2. DIC Budget

We now explore the cause of the DIC changes and associated CO_2 flux changes using a budget analysis for DIC at the ocean surface. The rate of change of DIC is defined by both physical processes and biological source/sink terms as follows:

$$\frac{\partial \text{DIC}}{\partial t} = -\nabla \cdot (\mathbf{u} \text{ DIC}) + \frac{\partial}{\partial z} \left(\kappa \frac{\partial \text{DIC}}{\partial z} \right) + F_{\text{CO}_2} + R_{\text{C:N}} S_{\text{NO}_3} + S_{\text{C}} + V_{\text{CO}_2}, \quad (4)$$

where \mathbf{u} is a three-dimensional velocity field, κ is the vertical diffusivity, F_{CO_2} is the air-sea flux of CO_2 calculated by Equation 2, $R_{\text{C:N}}$ is the biological transformation ratio between carbon and nitrogen, and S_{NO_3} and S_{C} are the sources and sinks of soft tissue and calcium carbonate, respectively. V_{CO_2} is the virtual flux of CO_2 and represents the concentration diluted through freshwater flux. Virtual flux shows negligible differences between two runs when compared with other terms and, hence, is not analyzed. The terms in Equation 4 are calculated online at every time step, which allows us to close the budget (Figure S1 in Supporting Information S1); however, 5-day mean values are considered in the analysis (Figure S2 in Supporting Information S1).

The DIC budget analysis clearly shows that the differences in the supply of carbon through $\frac{\partial}{\partial z} \left(\kappa \frac{\partial \text{DIC}}{\partial z} \right)$ that includes vertical mixing, diffusive processes, and convection creates the DIC differences and the air-sea CO_2 flux (Figure 4). The vertical mixing increases DIC by providing carbon-rich water to the surface with a positive $\frac{\partial}{\partial z} \left(\kappa \frac{\partial \text{DIC}}{\partial z} \right)$. DIC is decreased in the RW simulation, indicating the reduced carbon supply by vertical mixing when the current-wind interaction is considered (Figure 4c). The spatially averaged vertical mixing term in RW is reduced by up to 21%. The difference in the vertical mixing term shows similar seasonal variability as found for the air-sea CO_2 exchange (Figure 2b), suggesting that the changes in CO_2 flux are largely driven by the changes in the supply of DIC by vertical mixing.

The advection and biological source/sink terms are also affected (Figures 4b and 4d), although their changes are smaller compared with those in the vertical mixing and CO_2 flux terms. In addition, the positive differences in advection and biological source/sink terms imply that these terms tend to make the DIC concentration higher in

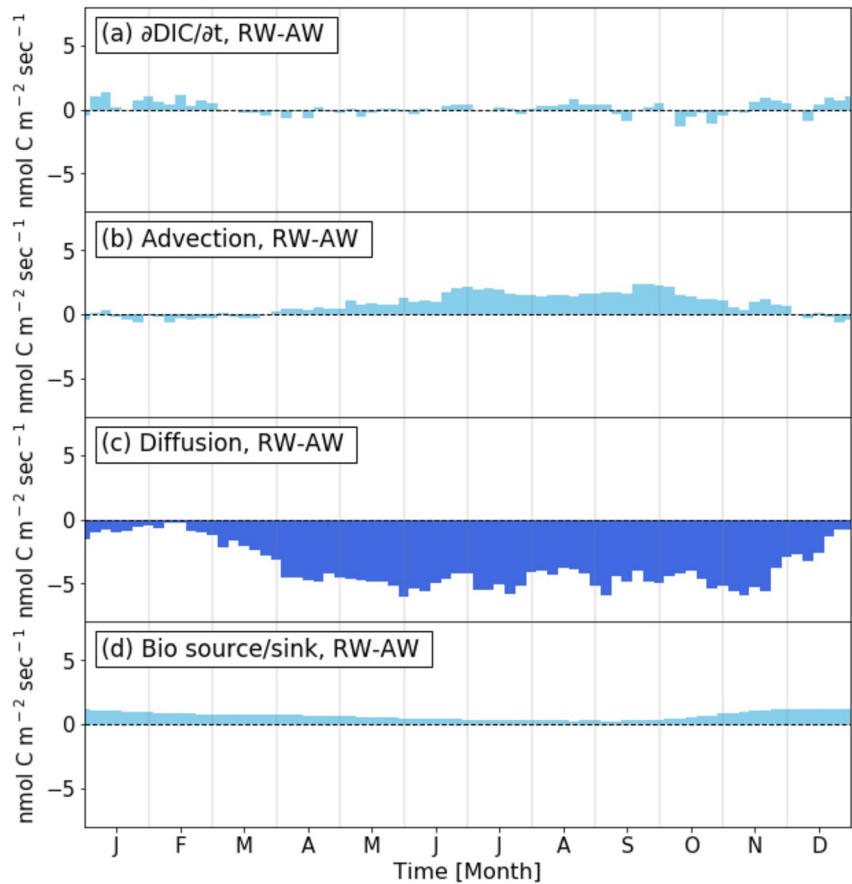


Figure 4. Differences between RW and AW (RW–AW) in (a) $\partial\text{DIC}/\partial t$, (b) advection, (c) diffusion (mixing), and (d) biological source/sink terms in the DIC budget analysis over the Pacific region of the model domain.

RW than in AW, which is contrary to the reduced $p\text{CO}_2$ results in the RW simulation compared to the AW simulation. For example, the change in the biological source/sink term suggests elevated biological activities in AW, leading to greater tendency to lower DIC concentration, particularly in spring and summer. However, the DIC concentration in the corresponding period is higher in AW than RW, which cannot be explained by biological activities. Hence, the advection and biological source/sink are not considered in the analysis.

The DIC budget analysis suggests that the weakening of the upward flux of carbon by vertical mixing is the primary reason for the lower DIC and $p\text{CO}_2$ and less wintertime CO_2 outgassing in the RW. The carbon supply by vertical mixing was computed using the vertical diffusivity (κ) and the vertical gradient of DIC. The latter is almost identical near the surface in the two simulations in winter. In contrast, the zonally averaged κ is larger in AW to the south of 55°S as inferred by the deeper mixing depth (Figure 5b). Hence, we argue that the lower level of DIC in RW originates from the weaker vertical mixing, which affects both $p\text{CO}_2$ and CO_2 outgassing. In the following subsection, we describe further analyses of the vertical cross section of DIC to explore the detailed processes from the smaller κ to lower DIC in RW.

4.3. Changes in the DIC Vertical Distribution by the Current-Wind Interaction

We found that the largest change in $p\text{CO}_2$ mainly occurred to the south of nSAF. This region includes the latitudinal band where westerly winds in the middle latitudes become polar easterlies. The northward and southward Ekman transports driven by the westerlies and easterlies, respectively, induce divergence near the surface and upwelling of carbon-rich water. The presence of sea-ice also triggers the effective divergence at the surface. The momentum transfer from the atmosphere to the ocean is reduced by sea-ice, and the equatorward Ekman transport occurs to the north of the sea-ice extent, providing a favorable condition for upwelling.

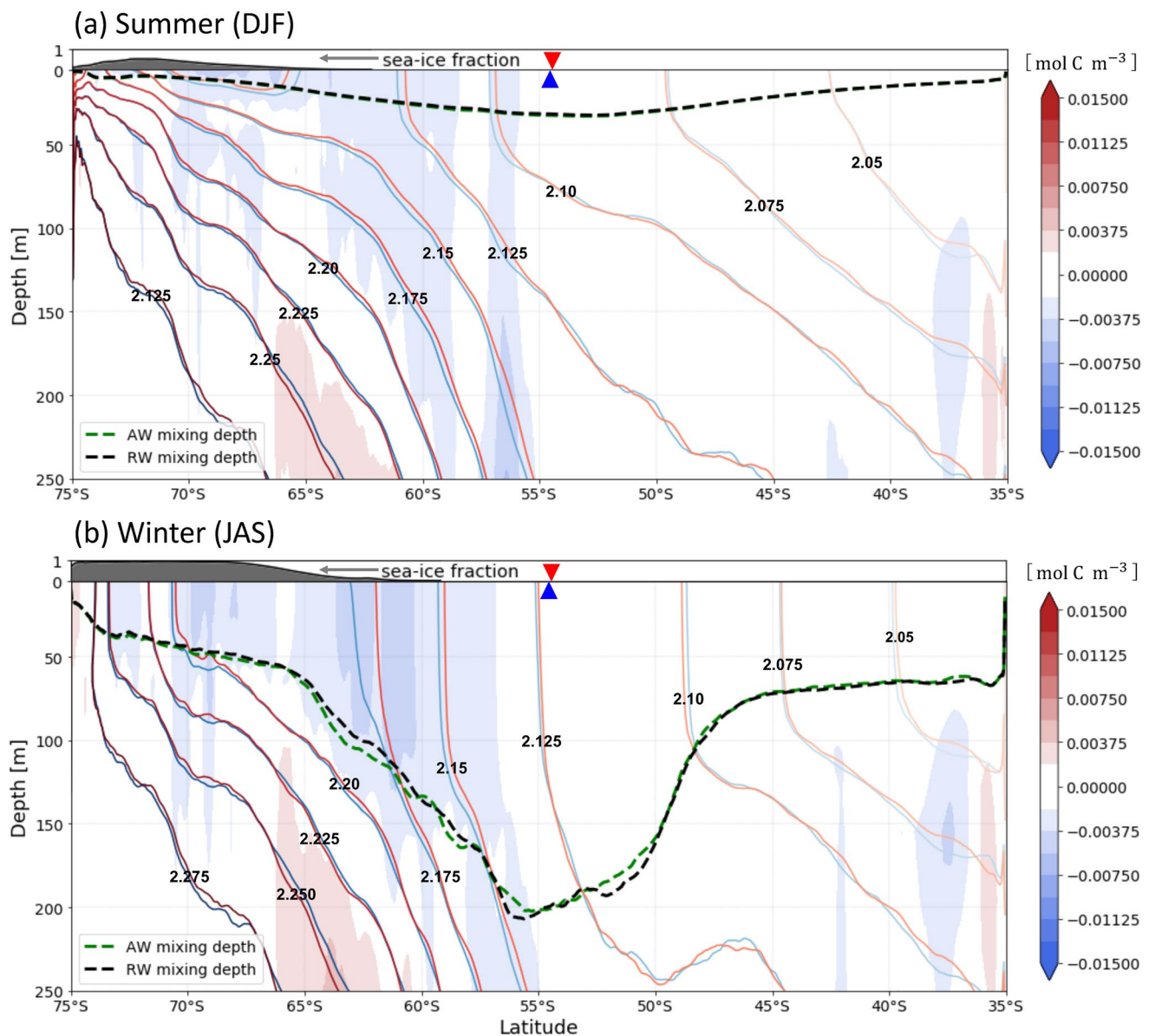


Figure 5. Averaged vertical structure during the winter (a) and summer (b). The solid lines indicate the DIC isopleth (red is the AW and blue is the RW). The dashed lines indicate the mixing depth. Triangles indicate the nSAF (red is the AW and blue is the RW). Shading indicates the DIC differences (RW-AW).

In summer, the DIC isopleths in RW are relatively deeper than those in AW, suggesting weaker upwelling (Figure 5a). This can reduce the chance of outcropping of DIC isopleths and the surface DIC concentration in RW. In fact, the reduction of DIC is the greatest in summer (Figure 3b), although it does not induce the largest changes in $p\text{CO}_2$ and CO_2 flux because of the dominance of the thermal component (Gruber et al., 2019). The mixing depth is confined within the top 20 m near the sea-ice extent in summer, making little impact on the DIC concentration. The DIC budget analysis also indicates the limited role of vertical mixing in causing the changes in DIC in summer (Figure 4c).

The wintertime DIC distributions show that the reduced DIC concentration to the south of nSAF in RW was due to the horizontal displacement of DIC isopleths (Figure 5b). The outcropping latitude of the DIC isopleth corresponding to 2.175 mol C m⁻³ in AW was near 61°S that is approximately 1° further north than found in RW. The DIC isopleths in both simulations under the sea-ice are indistinguishable and those to the north of 55°S are close to each other, which is consistent with the localized DIC changes observed with the current-wind interaction.

The reduced vertical mixing to the south of nSAF contributes to the lower DIC concentration in RW. Although the spatial mean mixing depth in AW and RW are similar; the AW simulation shows a slightly deeper mixing depth by up to roughly 10 m (dashed lines in Figure 5). This enhanced vertical mixing increases the DIC concentration at the surface. The lower DIC concentration in RW is confined within the mixing depth; the RW has a higher concentration of DIC than AW below the mixing depth near 65°S. This dipole pattern also suggests that the reduced vertical mixing in RW is the primary reason for the reduced DIC supply to the surface (Doddrige et al., 2021).

Weaker wintertime vertical mixing and upwelling in the RW are reinforced by the reduced upwelling in summer to result in a 17% reduction in the net CO₂ outgassing. The weaker wind stress and surface divergence to the south of nSAF place the DIC isopleths deeper than those in AW during spring and summer when the mixing depth occupies only top 10–20 m of the ocean. When the surface mixing intensifies and the DIC isopleths start to outcrop, these processes are delayed in RW compared with those in AW as the DIC isopleths are at a deeper level and vertical mixing is weaker. This possibly explains negligible DIC changes between the RW and AW in the subtropical ocean where the surface ocean is not preconditioned by upwelling of carbon-rich water in summer.

5. Discussion and Conclusion

The mechanical coupling through the current-wind interaction is capable of producing different both physical (e.g., decreased EKE) and biogeochemical ocean states compared to when this interaction is omitted. In this study, we investigate the changes in CO₂ flux due to the current-wind interaction in the Southern Ocean and their possible causes. We integrated two configurations of a high-resolution (1/20°) coupled physical-biogeochemical model near the Drake Passage in the Southern Ocean, in which the inclusion of the current-wind interaction is the only difference and analyzed the CO₂ flux changes using DIC budget analysis.

The comparison of the absolute wind (AW, no consideration of surface current in the calculation of wind stress) and relative wind (RW, inclusion of surface current in the calculation of wind stress) simulations show sizable differences in air-sea CO₂ exchange in the Southern Ocean, mainly stemming from the reduced *p*CO₂ in RW. The current-wind interaction reduced the contribution of the non-thermal component, DIC, to *p*CO₂ all year round, resulting in less outgassing in winter and more uptake in spring. Although the *p*CO₂ changes particularly stand out in winter, the decrease in DIC concentration in RW is greater in summer. However, differences in the SST limit the *p*CO₂ change in summer, as the thermal component is more important in this period. The annual integration of CO₂ flux suggests the net outgassing of 0.067 GtC with the current-wind interaction, which is 17% less than that in AW.

The air-sea CO₂ exchanges in the subtropical gyre region are similar in RW and AW, which is consistent with the previous study (Eden & Dietze, 2009) but becomes distinct to the south of northern Subantarctic Front (nSAF) as depicted in Figure 6. In this region, the DIC isopleths outcrop, creating a direct pathway for exchanges between the surface ocean and subsurface that is relatively rich in DIC. In RW, the outcropping latitudes are south of those in AW, indicating weaker Ekman transport due to reduced wind stress (dashed arrows in Figure 6). Weaker wind stress and reduced upwelling in RW also modify the DIC distribution in the interior oceans. The DIC isopleths are positioned at a slightly greater depth in RW, thereby reducing the upward flux compared with that in AW with similar size of surface vertical mixing, which is the case in summer. The DIC budget analysis indicated that the vertical displacement of the DIC isopleths to a shallower depth in RW preconditions the reduced DIC supply by vertical mixing in winter. These contributions from reduced upwelling and weaker vertical mixing reinforce each other to reduce the net CO₂ outgassing.

The DIC budget analysis also suggested systematic reduction of DIC consumption by biological activities with current-wind interaction. The Southern Ocean is a high-nutrient low-chlorophyll environment where the iron supply can promote primary production with sufficient solar irradiance. As vertical mixing is one of the important processes in supplying iron, the weaker vertical mixing in the RW in winter lowers the iron vertical flux, leading to less biological activity and less DIC consumption as solar irradiance increases in spring and the mixing depth shoals. Although this tends to elevate the DIC concentration in RW, its size is smaller than the change induced by vertical mixing, and *p*CO₂ changes follow the SST differences in two simulations.

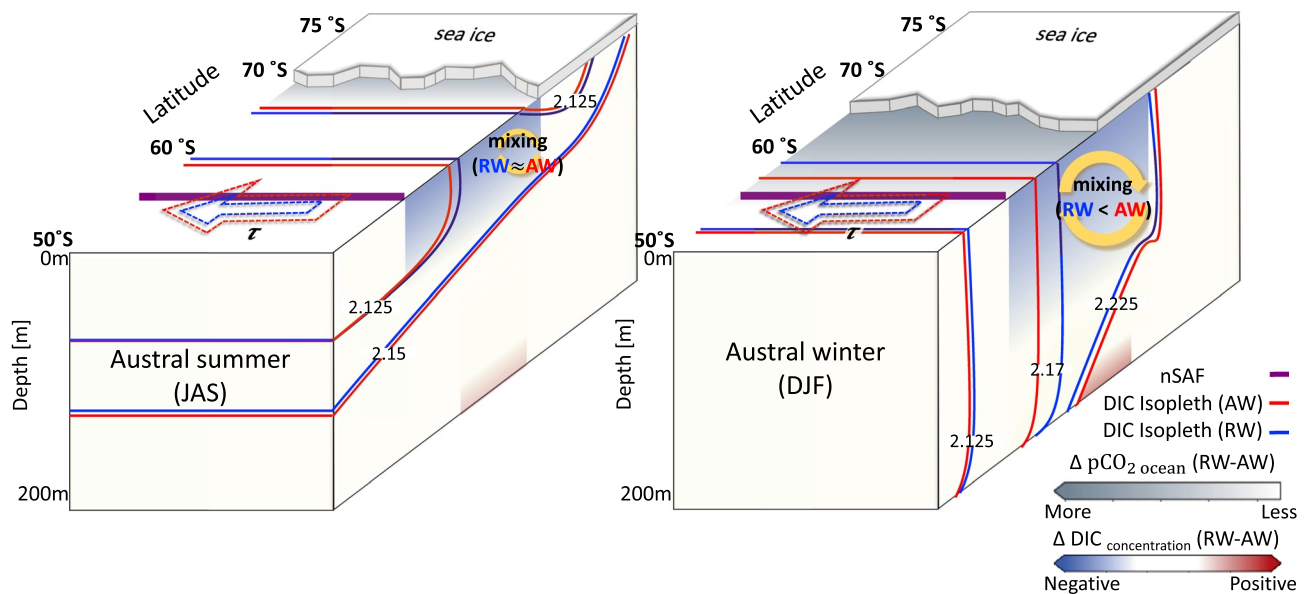


Figure 6. Schematic diagram depicting the effect of DIC concentration on the surface $p\text{CO}_2$ for the Pacific sector of the Southern Ocean. The westerlies wind stress is indicated by dashed lines (red is the AW and blue is the RW), the purple solid line is the nSAF, the gray shading at the surface shows $p\text{CO}_2$ differences (RW–AW), and the red to blue shading shows DIC differences (RW–AW).

Although we find the sizable changes in the air-sea CO_2 exchange by the current-wind interaction, there are notable limitations in the study. The current-wind interaction can affect the air-sea CO_2 exchange by modifying both the piston velocity and $p\text{CO}_2$, but the piston velocity was fixed in our experiment. The impact of SST perturbation on the surface wind, as well as the modulation of the surface wind by ocean current (Renault et al., 2016), can also adjust the piston velocity, which is not considered in our study. Additionally, Renault et al. (2016) note that the wind response to the current results in a partial re-energization of the ocean currents, suggesting that expressing the relative wind effect using α in Equation 3 is an oversimplification. Hence, it is necessary to investigate CO_2 flux exchanges more accurately using the coupled eddy-resolving ocean-atmosphere model with a biogeochemical model, which fully implemented the RW effect in the biogeochemical processes.

In our study area upstream of the Drake Passage over the Pacific, the latitudes of the wintertime intense vertical mixing are found near 55°S , which is farthest to the south than other ocean basins. This provides a favorable condition for DIC changes because the reduced upwelling and vertical mixing reinforce each other to the south of nSAF. However, this may not be the case in the Atlantic Ocean, which lacks intense wintertime vertical mixing, and in the Indian Ocean where the deep MLD is separated from the sea-ice extent region with stronger upwelling. Hence, it would be worthwhile to investigate whether and how the current-wind interaction can modify the air-sea CO_2 exchange in other basins.

Nevertheless, our study suggests that if the current-wind interaction is ignored in the model simulation, the $p\text{CO}_2$ can be overestimated to the south of nSAF in the Southern Ocean due to excessive upwelling and vertical mixing. This means that the Southern Ocean would be less effective in lowering $p\text{CO}_2$ in the atmosphere by both outgassing more carbon in winter or taking up less carbon in spring. This change in air-sea CO_2 exchange is significant considering only the south of nSAF contributes to this change with the undetectable difference in CO_2 in the mid-latitude. The full examination of the effect of air-sea interactions on the carbon exchange will be followed.

References

- Abernathy, R., Cerovecki, I., Holland, P., Newsom, E., Mazloff, M., & Talley, L. D. (2016). Water-mass transformation by sea ice in the upper branch of the Southern Ocean overturning. *Nature Geoscience*, 9(8), 596–601. <https://doi.org/10.1038/ngeo2749>
- Adcroft, A., Hill, C., Campin, J. M., Marshall, J., & Heimbach, P. (2004). Overview of the formulation and numerics of the MIT GCM. In *Proceedings of the ECMWF seminar series on numerical methods, recent developments in numerical methods for atmosphere and ocean modelling* (pp. 139–149). ECMWF. <https://www.ecmwf.int/node/7642>
- Adcroft, A., Hill, C., & Marshall, J. (1997). Representation of topography by shaved cells in a height coordinate ocean model. *Monthly Weather Review*, 125, 2293–2315. [https://doi.org/10.1175/1520-0493\(1997\)125<2293:rotbsc>2.0.co;2](https://doi.org/10.1175/1520-0493(1997)125<2293:rotbsc>2.0.co;2)

Acknowledgments

Some finds of this research are extracted from part of Kyungmin Kwak M.S. thesis. The MITgcm is available at <http://mitgcm.org>. This work was supported by the National Supercomputing Center with supercomputing resources including technical support (KSC-2020-CRE-0044). Kyungmin Kwak and Hajoong Song acknowledge the support from a National Research Foundation of Korea (NRF) grant funded by the Korean government (MSIT) (NRF-2019R1C1C1003663). Dennis J. McGillicuddy Jr. gratefully acknowledges support of the National Science Foundation and the National Aeronautics and Space Administration. Hyodae Seo thanks the support from the NSF (OCE-2022846), the NOAA (NA19OAR4310376), and the Andrew W. Mellon Foundation Endowed Fund for Innovative Research at WHOI. John Marshall acknowledges support from the Physical Oceanography program of NASA.

- Allison, L. C., Johnson, H. L., & Marshall, D. P. (2011). Spin-up and adjustment of the Antarctic circumpolar current and global pycnocline. *Journal of Marine Research*, 69(2–3), 167–189. <https://doi.org/10.1357/002224011798765330>
- Anderson, L. A., McGillicuddy, D. J., Maltrud, M. E., Lima, I. D., & Doney, S. C. (2011). Impact of eddy–wind interaction on eddy demographics and phytoplankton community structure in a model of the North Atlantic Ocean. *Dynamics of Atmospheres and Oceans*, 52(1–2), 80–94. <https://doi.org/10.1016/j.dynatmoce.2011.01.003>
- Anderson, L. A., & Robinson, A. R. (2001). Physical and biological modeling in the Gulf Stream region: Part II. Physical and biological processes. *Deep Sea Research Part I: Oceanographic Research Papers*, 48(5), 1139–1168. [https://doi.org/10.1016/S0967-0637\(00\)00092-3](https://doi.org/10.1016/S0967-0637(00)00092-3)
- Bakker, D. C. E., De Baar, H. J. W., & Bathmann, U. V. (1997). Changes of carbon dioxide in surface waters during spring in the Southern Ocean. *Deep-Sea Research Part II: Topical Studies in Oceanography*, 44(1–2), 91–127. [https://doi.org/10.1016/S0967-0645\(96\)00075-6](https://doi.org/10.1016/S0967-0645(96)00075-6)
- Belmonte Rivas, M., & Stoffelen, A. (2019). Characterizing ERA-Interim and ERA5 surface wind biases using ASCAT. *Ocean Science*, 15(3), 831–852. <https://doi.org/10.5194/os-15-831-2019>
- Brix, H., Currie, K. I., & Mikaloff Fletcher, S. E. (2013). Seasonal variability of the carbon cycle in subantarctic surface water in the South West Pacific. *Global Biogeochemical Cycles*, 27, 200–211. <https://doi.org/10.1002/gbc.20023>
- Carranza, M. M., & Gille, S. T. (2015). Southern Ocean wind-driven entrainment enhances satellite chlorophyll-a through the summer. *Journal of Geophysical Research*, 120(1), 304–323. <https://doi.org/10.1002/2014JC010203>
- Chelton, D. B., Schlax, M. G., & Samelson, R. M. (2007). Summertime coupling between sea surface temperature and wind stress in the California current system. *Journal of Physical Oceanography*, 37(3), 495–517. <https://doi.org/10.1175/JPO3025.1>
- Dee, D. P., Uppala, S. M., Simmons, A. J., Berrisford, P., Poli, P., Kobayashi, S., et al. (2011). The ERA-Interim reanalysis: Configuration and performance of the data assimilation system. *Quarterly Journal of the Royal Meteorological Society*, 137(656), 553–597. <https://doi.org/10.1002/qj.828>
- Dawe, J. T., & Thompson, L. (2006). Effect of ocean surface currents on wind stress, heat flux, and wind power input to the ocean. *Geophysical Research Letters*, 33(9). <https://doi.org/10.1029/2006GL025784>
- Dewar, W. K., & Flierl, G. R. (1987). Some effects of the wind on rings. *Journal of Physical Oceanography*, 17(10), 1653–1667. [https://doi.org/10.1175/1520-0485\(1987\)017<1653:seotwo>2.0.co;2](https://doi.org/10.1175/1520-0485(1987)017<1653:seotwo>2.0.co;2)
- Doddridge, E. W., Marshall, J., Song, H., Campin, J. M., & Kelley, M. (2021). Southern ocean heat storage, reemergence, and winter sea ice decline induced by summertime winds. *Journal of Climate*, 34(4), 1403–1415. <https://doi.org/10.1175/jcli-d-20-0322.1>
- Duhaut, T. H. A., & Straub, D. N. (2006). Wind stress dependence on ocean surface velocity: Implications for mechanical energy input to ocean circulation. *Journal of Physical Oceanography*, 36(2), 202–211. <https://doi.org/10.1175/JPO2842.1>
- Durack, P. J., Gleckler, P. J., Landerer, F. W., & Taylor, K. E. (2014). Quantifying underestimates of long-term upper-ocean warming. *Nature Climate Change*, 4(11), 999–1005. <https://doi.org/10.1038/nclimate2389>
- Dutkiewicz, S., Sokolov, A., Scott, J., & Stone, P. (2005). A three-dimensional ocean-sea-ice-carbon cycle model and its coupling to a two-dimensional atmospheric model: Uses in climate change studies. In *Joint program on the science policy global change. (chap. Rep. 122)*. MIT. <http://hdl.handle.net/1721.1/18091>
- Eden, C., & Dietze, H. (2009). Effects of mesoscale eddy/wind interactions on biological new production and eddy kinetic energy. *Journal of Geophysical Research*, 114(C5). <https://doi.org/10.1029/2008JC005129>
- Flierl, G. R., & Davis, C. S. (1993). Biological effects of Gulf Stream meandering. *Journal of Marine Research*, 51(3), 529–560. <https://doi.org/10.1357/0022240933224016>
- Forget, G. (2010). Mapping ocean observations in a dynamical framework: A 2004–06 ocean atlas. *Journal of Physical Oceanography*, 40(6), 1201–1221. <https://doi.org/10.1175/2009JPO4043.1>
- Frölicher, T. L., Sarmiento, J. L., Paynter, D. J., Dunne, J. P., Krasting, J. P., & Winton, M. (2015). Dominance of the Southern Ocean in anthropogenic carbon and heat uptake in CMIP5 models. *Journal of Climate*, 28(2), 862–886. <https://doi.org/10.1175/JCLI-D-14-00117.1>
- Gaube, P., Chelton, D. B., Samelson, R. M., Schlax, M. G., & O'Neill, L. W. (2015). Satellite observations of mesoscale eddy-induced ekman pumping. *Journal of Physical Oceanography*, 45(1), 104–132. <https://doi.org/10.1175/JPO-D-14-0032.1>
- Gray, A. R., Johnson, K. S., Bushinsky, S. M., Riser, S. C., Russell, J. L., Talley, L. D., et al. (2018). Autonomous biogeochemical floats detect significant carbon dioxide outgassing in the high-latitude southern ocean. *Geophysical Research Letters*, 45, 9049–9057. <https://doi.org/10.1029/2018GL078013>
- Gregor, L., Kok, S., & Monteiro, P. M. S. (2018). Interannual drivers of the seasonal cycle of CO₂ in the Southern Ocean. *Biogeosciences*, 15(8), 2361–2378. <https://doi.org/10.5194/bg-15-2361-2018>
- Gruber, N., Landschützer, P., & Lovenduski, N. S. (2019). The variable Southern Ocean carbon sink. *Annual Review of Marine Science*, 11(1), 159–186. <https://doi.org/10.1146/annurev-marine-121916-063407>
- Hales, B., & Takahashi, T. (2004). High-resolution biogeochemical investigation of the Ross Sea, Antarctica, during the AESOPS (U. S. JGOFS) Program. *Global Biogeochemical Cycles*, 18(3). <https://doi.org/10.1029/2003GB002165>
- Huang, R. X., Wang, W., & Liu, L. L. (2006). Decadal variability of wind-energy input to the world ocean. *Deep Sea Research Part II: Topical Studies in Oceanography*, 53(1–2), 31–41. <https://doi.org/10.1016/j.dsr2.2005.11.001>
- Hutchinson, D. K., Hogg, A. M. C., & Blundell, J. R. (2010). Southern ocean response to relative velocity wind stress forcing. *Journal of Physical Oceanography*, 40(2), 326–339. <https://doi.org/10.1175/2009JPO4240.1>
- Jullien, S., Masson, S., Oerder, V., Samson, G., Colas, F., & Renault, L. (2020). Impact of Ocean-Atmosphere Current Feedback on Ocean Mesoscale Activity: Regional Variations and Sensitivity to Model Resolution. *Journal of Climate*, 33(7), 2585–2602. <https://doi.org/10.1175/JCLI-D-19-0484.1>
- Khatiwala, S., Primeau, F., & Hall, T. (2009). Reconstruction of the history of anthropogenic CO₂ concentrations in the ocean. *Nature*, 462, 346–349. <https://doi.org/10.1038/nature08526>
- Langlais, C. E., Rintoul, S. R., & Zika, J. D. (2015). Sensitivity of antarctic circumpolar current transport and eddy activity to wind patterns in the Southern Ocean. *Journal of Physical Oceanography*, 45(4), 1051–1067. <https://doi.org/10.1175/JPO-D-14-0053.1>
- Large, W., McWilliams, J., & Doney, S. (1994). Oceanic vertical mixing: A review and a model with a nonlocal boundary layer parameterization. *Reviews of Geophysics*, 32, 363–403. <https://doi.org/10.1029/94RG01872>
- Large, W. G., & Yeager, S. G. (2004). *Diurnal to decadal global forcing for ocean and sea-ice models: The data sets and flux climatologies (NCAR, Tech. Rep.)*. National Center for Atmospheric Research Boulder. <https://doi.org/10.5065/D6KK98Q6>
- Ledwell, J. R., McGillicuddy, D., Jr., & Anderson, L. A. (2008). Nutrient flux into an intense deep chlorophyll layer in a mode-water eddy. *Deep Sea Research Part II: Topical Studies in Oceanography*, 55(10–13), 1139–1160. <https://doi.org/10.1016/j.dsr2.2008.02.005>
- Lenton, A., Matear, R. J., & Tilbrook, B. (2006). Design of an observational strategy for quantifying the Southern Ocean uptake of CO₂. *Global Biogeochemical Cycles*, 20(4), 20. <https://doi.org/10.1029/2005GB002620>

- Lenton, A., Tilbrook, B., Law, R. M., Bakker, D., Doney, S. C., Gruber, N., et al. (2013). Sea-air CO₂ fluxes in the Southern Ocean for the period 1990–2009. *Biogeosciences*, *10*(6), 4037–4054. <https://doi.org/10.5194/bg-10-4037-2013>
- Le Quéré, C., Andrew, R. M., Friedlingstein, P., Sitch, S., Hauck, J., Pongratz, J., et al. (2018). Global carbon budget 2018. *Earth System Science Data*, *10*(4), 2141–2194. <https://doi.org/10.5194/essd-10-2141-2018>
- Lévy, M., Franks, P. J., & Smith, K. S. (2018). The role of submesoscale currents in structuring marine ecosystems. *Nature Communications*, *9*(1). <https://doi.org/10.1038/s41467-018-07059-3>
- Lévy, M., Klein, P., & Treguier, A.-M. (2001). Impact of sub-mesoscale physics on production and subduction of phytoplankton in an oligotrophic regime. *Journal of Marine Research*, *59*(4), 535–565. <https://doi.org/10.1357/002224001762842181>
- Liang, X., Spall, M., & Wunsch, C. (2017). Global ocean vertical velocity from a dynamically consistent ocean state estimate. *Journal of Geophysical Research*, *122*(10), 8208–8224. <https://doi.org/10.1002/2017JC012985>
- Llovel, W., & Terray, L. (2016). Observed southern upper-ocean warming over 2005–2014 and associated mechanisms. *Environmental Research Letters*, *11*(12), 124023. <https://doi.org/10.1088/1748-9326/11/12/124023>
- Losch, M., Menemenlis, D., Campin, J. M., Heimbach, P., & Hill, C. (2010). On the formulation of sea-ice models. Part 1: Effects of different solver implementations and parameterizations. *Ocean Modelling*, *33*(1–2), 129–144. <https://doi.org/10.1016/j.ocemod.2009.12.008>
- Luis, A. J., & Pandey, P. C. (2004). Seasonal variability of QSCAT-derived wind stress over the Southern Ocean. *Geophysical Research Letters*, *31*(13). <https://doi.org/10.1029/2003GL019355>
- Luo, C., Mahowald, N., Bond, T., Chuang, P. Y., Artaxo, P., Siefert, R., et al. (2008). Combustion iron distribution and deposition. *Global Biogeochemical Cycles*, *22*(1). <https://doi.org/10.1029/2007GB002964>
- Mahadevan, A., & Archer, D. (2000). Modeling the impact of fronts and mesoscale circulation on the nutrient supply and biogeochemistry of the upper ocean. *Journal of Geophysical Research*, *105*(C1), 1209–1225. <https://doi.org/10.1029/1999JC900216>
- Marshall, J., Adcroft, A., Hill, C., Perelman, L., & Heisey, C. (1997). A finite-volume, incompressible Navier Stokes model for studies of the ocean on parallel computers. *Journal of Geophysical Research*, *102*(C3), 5753–5766. <https://doi.org/10.1029/96JC02775>
- Marshall, J., Hill, C., Perelman, L., & Adcroft, A. (1997). Hydrostatic, quasi-hydrostatic, and nonhydrostatic ocean modeling. *Journal of Geophysical Research*, *102*(C3), 5733–5752. <https://doi.org/10.1029/96JC02776>
- Marshall, J., Jones, H., & Hill, C. (1998). Efficient ocean modeling using non-hydrostatic algorithms. *Journal of Marine Systems*, *18*(1–3), 115–134. [https://doi.org/10.1016/S0924-7963\(98\)00008-6](https://doi.org/10.1016/S0924-7963(98)00008-6)
- Marshall, J., & Speer, K. (2012). Closure of the meridional overturning circulation through Southern Ocean upwelling. *Nature Geoscience*, *5*(3), 171–180. <https://doi.org/10.1038/ngeo1391>
- Martin, A. P., & Richards, K. J. (2001). Mechanisms for vertical nutrient transport within a North Atlantic mesoscale eddy. *Deep Sea Research Part II: Topical Studies in Oceanography*, *48*(4–5), 757–773. [https://doi.org/10.1016/S0967-0645\(00\)00096-5](https://doi.org/10.1016/S0967-0645(00)00096-5)
- McGillicuddy, D. J., Anderson, L. A., Bates, N. R., Bibby, T., Buesseler, K., Carlson, C., et al. (2007). Eddy/Wind interactions stimulate extraordinary mid-ocean plankton blooms. *Science*, *316*, 1021–1026. <https://doi.org/10.1126/science.1136256>
- Metz, N., Brunet, C., Jabaud-Jan, A., Poisson, A., & Schauer, B. (2006). Summer and winter air-sea CO₂ fluxes in the Southern Ocean. *Deep Sea Research Part I*, *53*(9), 1548–1563. <https://doi.org/10.1016/j.dsr.2006.07.006>
- Mikaloff Fletcher, S. E., Gruber, N., Jacobson, A. R., Doney, S. C., Dutkiewicz, S., Gerber, M., et al. (2006). Inverse estimates of anthropogenic CO₂ uptake, transport, and storage by the ocean. *Global Biogeochemical Cycles*, *20*(2). <https://doi.org/10.1029/2005GB002530>
- Morrison, A. K., Griffies, S. M., Winton, M., Anderson, W. G., & Sarmiento, J. L. (2016). Mechanisms of Southern Ocean heat uptake and transport in a global eddying climate model. *Journal of Climate*, *29*(6), 2059–2075. <https://doi.org/10.1175/JCLI-D-15-0579.1>
- Olsen, A., Lange, N., Key, R. M., Tanhua, T., Bittig, H. C., Kozyr, A., et al. (2020). GLODAPv2. 2020—the second update of GLODAPv2. *Earth System Science Data*. <https://doi.org/10.5194/essd-2020-165>
- Parekh, P., Follows, M. J., Dutkiewicz, S., & Ito, T. (2006). Physical and biological regulation of the soft tissue carbon pump. *Paleoceanography*, *21*(3). <https://doi.org/10.1029/2005PA001258>
- Person, R., Aumont, O., & Lévy, M. (2018). The biological pump and seasonal variability of pCO₂ in the Southern Ocean: Exploring the role of diatom adaptation to low iron. *Journal of Geophysical Research*, *123*(5), 3204–3226. <https://doi.org/10.1029/2018JC013775>
- Pezzi, L. P., de Souza, R. B., Santini, M. F., Miller, A. J., Carvalho, J. T., Parise, C. K., et al. (2021). Oceanic eddy-induced modifications to air-sea heat and CO₂ fluxes in the Brazil-malvinas confluence. *Scientific Reports*, *11*(1), 10648. <https://doi.org/10.1038/s41598-021-89985-9>
- Putrasahan, D. A., Miller, A. J., & Seo, H. (2013). Regional coupled ocean-atmosphere downscaling in the Southeast Pacific: Impacts on upwelling, mesoscale air-sea fluxes, and ocean eddies. *Ocean Dynamics*, *63*, 463–488. <https://doi.org/10.1007/s10236-013-0608-2>
- Renault, L., Molemaker, M. J., McWilliams, J. C., Shchepetkin, A. F., Lemarié, F., Chelton, D., et al. (2016). Modulation of wind work by oceanic current interaction with the atmosphere. *Journal of Physical Oceanography*, *46*(6), 1685–1704. <https://doi.org/10.1175/JPO-D-15-0232.1>
- Roemmich, D., Church, J., Gilson, J., Monselesan, D., Sutton, P., & Wijffels, S. (2015). Unabated planetary warming and its ocean structure since 2006. *Nature Climate Change*, *5*(3), 240–245. <https://doi.org/10.1038/nclimate2513>
- Sallée, J.-B. (2018). Southern Ocean warming. *Oceanography*, *31*(2), 52–62. <https://doi.org/10.5670/oceanog.2018.215>
- Samelson, R. M., Skillingstad, E. D., Chelton, D. B., Esbensen, S. K., O'Neill, L. W., & Thum, N. (2006). On the coupling of wind stress and sea surface temperature. *Journal of Climate*, *19*(8), 1557–1566. <https://doi.org/10.1175/JCLI3682.1>
- Seo, H. (2017). Distinct influence of air-sea interactions mediated by mesoscale sea surface temperature and surface current in the Arabian Sea. *Journal of Climate*, *30*(20), 8061–8080. <https://doi.org/10.1175/JCLI-D-16-0834.1>
- Seo, H., Miller, A. J., & Norris, J. R. (2016). Eddy-wind interaction in the California current system: Dynamics and impacts. *Journal of Physical Oceanography*, *46*(2), 439–459. <https://doi.org/10.1175/JPO-D-15-0086.1>
- Seo, H., Miller, A. J., & Roads, J. O. (2007). The Scripps Coupled Ocean-Atmosphere Regional (SCOAR) model, with applications in the eastern Pacific sector. *Journal of Climate*, *20*(3), 381–402. <https://doi.org/10.1175/JCLI4016.1>
- Seo, H., Subramanian, A. C., Song, H., & Chowdary, J. S. (2019). Coupled effects of ocean current on wind stress in the Bay of Bengal: Eddy energetics and upper ocean stratification. *Deep Sea Research Part II: Topical Studies in Oceanography*, *168*, 104617. <https://doi.org/10.1016/j.dsr2.2019.07.005>
- Smith, C. L., Richards, K. J., & Fasham, M. J. R. (1996). The impact of mesoscale eddies on plankton dynamics in the upper ocean. *Deep Sea Research Part I: Oceanographic Research Papers*, *43*(11–12), 1807–1832. [https://doi.org/10.1016/S0967-0637\(96\)00035-0](https://doi.org/10.1016/S0967-0637(96)00035-0)
- Song, H., Marshall, J., Follows, M. J., Dutkiewicz, S., & Forget, G. (2016). Source waters for the highly productive Patagonian shelf in the southwestern Atlantic. *Journal of Marine Systems*, *158*, 120–128. <https://doi.org/10.1016/j.jmarsys.2016.02.009>
- Song, H., Marshall, J., McGillicuddy, D., & Seo, H. (2020). Impact of current-wind interaction on vertical processes in the Southern Ocean. *Journal of Geophysical Research*, *125*, e2020JC016046. <https://doi.org/10.1029/2020JC016046>
- Song, H., Marshall, J., Munro, D. R., Dutkiewicz, S., Sweeney, C., McGillicuddy, D. J., Jr, et al. (2016). Mesoscale modulation of air-sea CO₂ flux in Drake passage. *Journal of Geophysical Research*, *121*, 6635–6649. <https://doi.org/10.1002/2016JC011714>

- Takahashi, T., Sutherland, S. C., Sweeney, C., Poisson, A., Metzl, N., Tilbrook, B., et al. (2002). Global sea-air CO₂ flux based on climatological surface ocean pCO₂, and seasonal biological and temperature effects. *Deep Sea Research Part II*, 49(9–10), 1601–1622. [https://doi.org/10.1016/S0967-0645\(02\)00003-6](https://doi.org/10.1016/S0967-0645(02)00003-6)
- Takahashi, T., Sutherland, S. C., Wanninkhof, R., Sweeney, C., Feely, R. A., Chipman, D. W., et al. (2009). Climatological mean and decadal change in surface ocean pCO₂, and net sea-air CO₂ flux over the global oceans. *Deep-Sea Research Part II*, 56(8–10), 554–577. <https://doi.org/10.1016/j.dsr2.2008.12.009>
- Takahashi, T., Sweeney, C., Hales, B., Chipman, D. W., Newberger, T., Goddard, J. G., et al. (2012). The changing carbon cycle in the Southern Ocean. *Oceanography*, 25(3), 26–37. <https://doi.org/10.5670/oceanog.2012.71>
- Tamsitt, V., Drake, H. F., Morrison, A. K., Talley, L. D., Dufour, C. O., Gray, A. R., et al. (2017). Spiraling pathways of global deep waters to the surface of the Southern Ocean. *Nature Communications*, 8(1). <https://doi.org/10.1038/s41467-017-00197-0>
- Thomalla, S. J., Fauchereau, N., Swart, S., & Monteiro, P. M. S. (2011). Regional scale characteristics of the seasonal cycle of chlorophyll in the Southern Ocean. *Biogeosciences*, 8, 2849–2866. <https://doi.org/10.5194/bg-8-2849-2011>
- Verdy, A., Dutkiewicz, S., Follows, M. J., Marshall, J., & Czaja, A. (2007). Carbon dioxide and oxygen fluxes in the Southern Ocean: Mechanisms of interannual variability. *Global Biogeochemical Cycles*, 21(2). <https://doi.org/10.1029/2006GB002916>
- Wang, Z., Kuhlbrodt, T., & Meredith, M. P. (2011). On the response of the antarctic circumpolar current transport to climate change in coupled climate models. *Journal of Geophysical Research*, 116(C8). <https://doi.org/10.1029/2010JC006757>
- Wanninkhof, R. (1992). Relationship between wind speed and gas exchange over the ocean. *Journal of Geophysical Research*, 97(C5), 7373–7382. <https://doi.org/10.1029/92JC00188>
- Wu, Y., Hain, M. P., Humphreys, M. P., Hartman, S., & Tyrrell, T. (2019). What drives the latitudinal gradient in open-ocean surface dissolved inorganic carbon concentration? *Biogeosciences*, 16(13), 2661–2681. <https://doi.org/10.5194/bg-16-2661-2019>
- Wunsch, C. (1998). The work done by the wind on the oceanic general circulation. *Journal of Physical Oceanography*, 28(11), 2332–2340. [https://doi.org/10.1175/1520-0485\(1998\)028<2332:twdbtw>2.0.co;2](https://doi.org/10.1175/1520-0485(1998)028<2332:twdbtw>2.0.co;2)
- Yoshimori, A., & Kishi, M. J. (1994). Effects of interaction between two warm-core rings on phytoplankton distribution. *Deep Sea Research Part I: Oceanographic Research Papers*, 41(7), 1039–1052. [https://doi.org/10.1016/0967-0637\(94\)90017-5](https://doi.org/10.1016/0967-0637(94)90017-5)
- Zhai, X., & Greatbatch, R. J. (2007). Wind work in a model of the northwest Atlantic Ocean. *Geophysical Research Letters*, 34(4). <https://doi.org/10.1029/2006GL028907>
- Zhai, X., Johnson, H. L., Marshall, D. P., & Wunsch, C. (2012). On the wind power input to the ocean general circulation. *Journal of Physical Oceanography*, 42(8), 1357–1365. <https://doi.org/10.1175/JPO-D-12-09.1>